NUCL SCI TECH (2017) 28:80
DOI 10.1007/s41365-017-0236-5

Feasibility study on determining the conventional true value of gamma-ray air kerma in a minitype reference radiation

Yi-Xin Liu[1,2] · Biao Wei[1] · Yang Xu[1,2] · Meng He[2] · Ren-Hong Zhuo[2] · De-Zhi Wen[2] · Da-Jie Ding[2] · Ben-Jiang Mao[2]

Received: 14 August 2015 / Revised: 9 October 2015 / Accepted: 29 October 2015 / Published online: 6 May 2017

Abstract A minitype reference radiation (MRR) with dimensions of only 1 m × 1 m × 1 m has been developed for the in situ calibration of photon dosimeters. The present work conducts a feasibility study on determining the conventional true value of gamma-ray air kerma at the point of test in the MRR. Owing to its smaller dimensions, the scattered gamma-rays in the MRR are expected to induce a non-negligible interference with the radiation field compared with conditions in the standard reference radiation stipulated by ISO4037-1 or GB/T12162.1. A gamma-ray spectrometer was employed to obtain the spectra of scattered gamma-rays within the MRR, and the feature components of the spectra were extracted by principal component analysis to characterize the interference of a dosimeter probe in the radiation field. A prediction model of the CAK at the point of test was built by least squares support vector machine based on the feature component data obtained from nine sample dosimeters under five different dose rates. The mean prediction error of the CAK prediction model was within ±4.5%, and the maximum prediction error was about ±10%.

Keywords Air kerma · Reference radiation · Calibration · Principal component analysis · Support vector machine

✉ Ben-Jiang Mao
liuyx123456789@126.com

[1] Key Laboratory of Optoelectronics Technology and System, Ministry of Education, Chongqing University, Chongqing 400044, China

[2] Institute of Nuclear Physics and Chemistry, China Academy of Engineering Physics, Mianyang 621999, China

1 Introduction

According to the JJG393-2003 or IEC60846 standard, all gamma-ray dosimeters serving the purpose of radiation protection must be regularly calibrated every year. At present, the calibration work must employ the standard reference radiation (SRR) stipulated by the ISO4037-1 or GB/T12162.1 standard. However, because the size of the SRR is 4 m × 4 m × 3 m or greater [1, 2], the calibration facility is not portable, and all dosimeters must therefore be transported yearly to a fixed facility for calibration. However, relatively fixed dosimeters installed within nuclear facilities cannot be conveniently transported to a fixed calibration facility, and should therefore be calibrated in situ, which is typically accomplished using the substitution method and a lower intensity source. However, dosimeter performance cannot be evaluated scientifically under this condition because the full dosimeter range cannot be covered and ambient scattering disturbances cannot be evaluated. Therefore, a mobile calibration installation employing a reference radiation that occupies a much smaller space is obviously necessary.

To develop a mobile calibration facility, a minitype reference radiation (MRR) is proposed, which reduces the SRR dimensions to 1 m × 1 m × 1 m. However, the much smaller size of the MRR produces non-negligible scattering of gamma-rays, which represents a crucial disturbance when attempting to determine the conventional true air kerma (CAK) value for gamma-rays [3]. Due to the varied probe sizes and energy responses of dosimeters, it is very difficult to determine the contribution of the scattering components accurately and thereby make corrections. Therefore, the CAK value obtained in the MRR is not equivalent to that obtained in an SRR stipulated by

ISO4037-1. In this article, a feasibility study on determining the CAK value in the MRR is carried out.

2 Methodology

The MRR is a cubic box of 1 m side length shielded by lead plates, as illustrated in Fig. 1. The geometric center of the MRR is defined as the point of test, at which the reference point of a dosimeter probe is positioned. In an SRR, the air kerma measured by a graphite cavity ionization chamber at the point of test can be used as the CAK in calibration work because the ambient scattered rays are strictly controlled to a very low level. However, due to the scattered gamma-rays arising from the inner surface of the MRR shielding and the outer surface of the dosimeter probe, and the secondary scattered rays, the air kerma value $Kaij'$ measured by a graphite cavity ionization chamber at the point of test in the MRR differs from the value obtained in an SRR. In fact, it is very difficult to discriminate between the contributions of source and scattered gamma-ray components to the CAK at the point of test in the MRR experimentally. In the present work, a gamma-ray spectrometer is employed to characterize the scattered gamma spectrum Sij, and we assume a functional relationship $Kaij = f(Sij,Kaij')$.

A series of sample dosimeters that we employ normally in our daily radiation protection work was selected for investigation using both the MRR and an SRR. When a dosimeter was position at the point of test in the MRR, the measured value was R. Then, we can explore a point at the SRR where the measured value of the meter was also R. The air kerma of the point in SRR can be used as the equivalent value of the CAK in the MRR because the dosimeter shared the same contribution to the measured value from different gamma-ray components. Therefore, the sample dosimeter is actually employed as a transfer tool that establishes connection between the SRR and the MRR for determining the value of $Kaij$ at the point of test in the MRR. Employing the above method with a series of sample dosimeters yields a series of data sets, including values of $Kaij$, Sij, and $Kaij'$. Then, least squares support vector machine (LS-SVM) is employed for the regression analysis of the data sets, and a prediction model of $Kaij$ based on the functional relationship $Kaij = f(Sij,Kaij')$ at the point of test in the MRR is built, which can be applied for predicting the value of $Kaij$ for a non-sample dosimeter or a dosimeter needing calibration in the MRR.

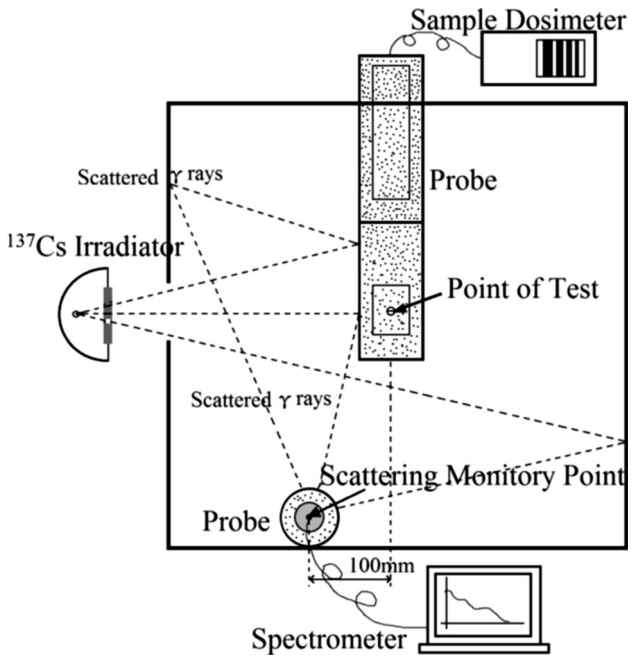

Fig. 1 Schematic of the MMR and experimental setup

The procedure employed for data processing and model training is given as follows.

1. Position sample dosimeter i, for $i = 1, 2, \ldots, x$, at the point of test of the MRR, and introduce gamma-ray intensities Ij, for $j = 1,2,\ldots,y$, for each sample dosimeter, which yields $x \times y$ sets of $Kaij'$, Sij, and $Kaij$.
2. Due to statistical fluctuations in the gamma-ray emission of the radioactive source and electronic noise, wavelet analysis is applied to denoise Sij [4].
3. Dispersing each line of Sij by a fixed gamma-ray energy separation E, we obtain an n-dimensional gamma-ray count rate array φijn, where n is the total number of gamma-ray count rate values.
4. A sample matrix $T(x \times y) \times n$ is constituted from the x sample dosimeters, y source intensities Ij, and the series φijn.
5. To reduce the dimensions of $T(x \times y) \times n$, principal component analysis (PCA) is applied to extract feature components Ψij [5, 6].
6. Finally, LS-SVM is employed to train the prediction model of $Kaij$ based on Ψij, which can be rewritten as $Kaij = f(\Psi ij,Kaij')$.

The procedure for constructing the $Kaij$ prediction model is outlined formally in Fig. 2, and the procedure for the extraction of Ψij using PCA is outlined in Fig. 3.

3 Experimental installation

As discussed above, the MRR represents an enclosed gamma-ray field within a cubic shielding box with 1 m side lengths, which is shielded by lead plates. Their radiator for gamma-ray injection was installed on the one side of the shielding box via a 120-mm-diameter circular hole. During

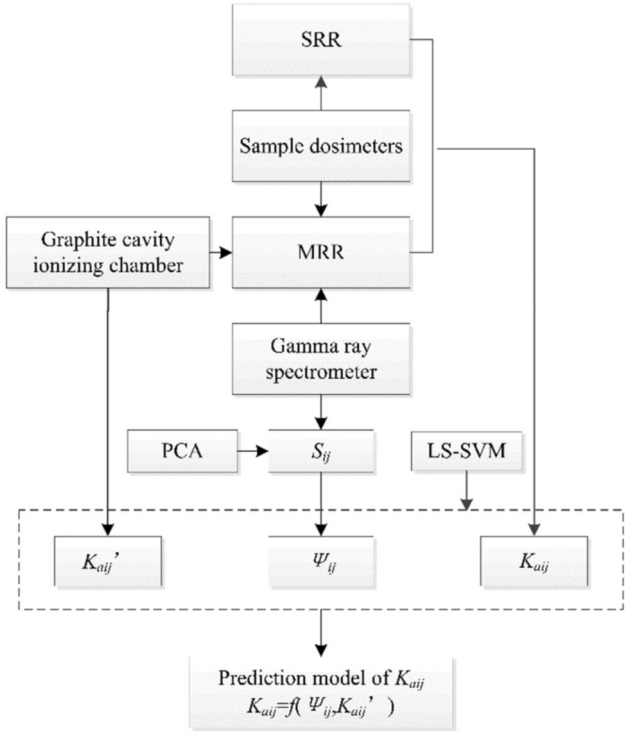

Fig. 2 Procedure for constructing the *Kaij* prediction model based on the functional form $K_{aij} = f(\Psi_{ij}, K_{aij}')$ employing principal component analysis (PCA) to extract feature components Ψ_{ij} and least squares support vector machine (LS-SVM) to train the prediction model

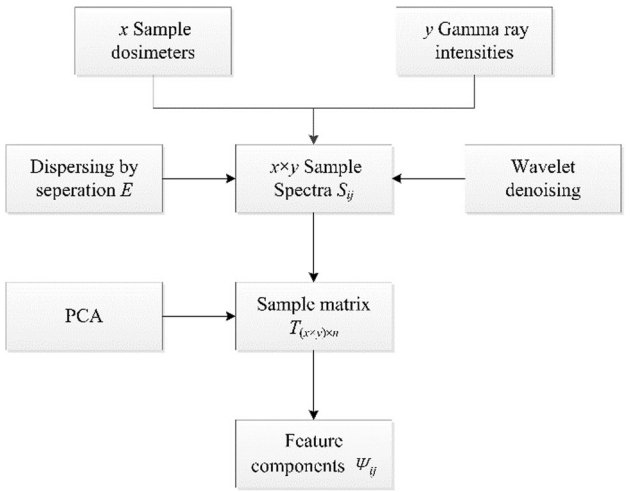

Fig. 3 Procedure for extracting feature components Ψ_{ij} using principal component analysis (PCA)

investigation, the probe of a sample dosimeter was mounted vertically from a circular hole on the top side of the shielding box. The reference point on the probe coincided with the point of test in the MRR. A scattering monitory point was labeled for positioning the probe of a gamma-ray spectrometer on the central line of the MRR's inner bottom, near the side of gamma-ray inlet and 100 mm away from the projection point of the point of test as illustrated in Fig. 1.

The experimental installation was built up on a calibration facility denoted as the gamma-ray air kerma (protection level) measurement standard, which is denoted here in simply as the standard installation. The facility belongs to the Ionizing Radiation Metrology Station, one of the subsidiaries of the China Academy of Engineering Physics. The gamma-rays in the MRR were irradiated horizontally at or of the standard installation with an activity of about 7.141×10^{10}Bq. Various attenuators from a cesium-137 isotope source in the irradiator were assembled on the outlet of the irradiator to investigate the intensity of the gamma-ray irradiation injected into the MRR. The MRR box was mounted on a small railcar for adjusting the distance between the outlet of their radiator and the inlet of the MRR box. An image of the experimental installation is presented in Fig. 4.

According to the regulated dose range of gamma-ray dosimeters employed for radiation protection, we selected five gamma-ray intensities *Ij* as five sources for investigation by employing different attenuators and adjusting the distance between the MRR inlet and their radiator outlet. The dose rates at the point of test corresponding to each source investigated are listed in Table 1. During investigation, a standard graphite cavity ionization chamber (PTW-32005, PTB, Germany) was employed to determine the air kerma of the point of test in the MRR. The scattered gamma spectrum at the scattering monitory point was measured by a portable gamma-ray spectrometer (modelInspector1000, Canberra, USA). Investigations were conducted using the nine sample gamma dosimeters listed in Table 2.

Fig. 4 (Color online) Image of the experimental mobile installation

Table 1 Dose rates investigated at the test point

Serial number of gamma-ray intensity	Source 1	Source 2	Source 3	Source 4	Source 5
Dose rate (μGy/h)	67.68	148.68	393.48	894.24	1215.72

Table 2 Sample dosimeters employed for investigation

No.	Model	Detector	Probe diameter(mm)	Manufacturer
1	BH3103A	NaI Crystal	93	Beijing Nuclear Instrument Factory, China
2	FJ317E	GM Tube	45	Xi'an Nuclear Instrument Factory, China
3	SSM-1(07-00362)	GM Tube	45	Austrian Research Centre Seibersdorf
4	SSM-1(03-107)	GM Tube	45	Austrian Research Centre Seibersdorf
5	FD-3013B	NaI Crystal	40	CNNC Shanghai Electronics Instrument Co., Ltd., China
6	CIT-2000FXγ	NaI Crystal	45	Sumstar Group Corp. China
7	Inspector 1000 (IPRON-3)	NaI Crystal	80	Canberra, USA
8	Inspector 1000 (IPROS-2)	NaI Crystal	60	Canberra, USA
9	Canberra Radiagem 2000	NaI Crystal	70	Canberra, USA

4 Results and discussion

4.1 Characteristics of scattered gamma-rays in the MRR

Owing to its smaller dimensions, the scattered gamma-rays in the MRR are expected to induce a more obvious interference with the radiation field compared with an SRR.

The gamma-ray spectra obtained from the nine sample dosimeters irradiated with source 5 are given in Fig. 5. A total of five characteristic peaks are observed for each spectrum at equivalent positions and with similar shapes for the different probes. The energies of all five characteristic peaks were less than 750 keV. The gamma-ray spectra obtained from the BH3103A dosimeter when respectively irradiated with the five sources are presented in Fig. 6. The peak positions and shapes of all spectra are nearly equivalent, except for those of peak 5. In addition, analysis reveals that the peak count rate increases almost linearly with increasing irradiation dose rate, particularly for peak 4. Therefore, we find that the positions of peaks 1–4 are nearly constant regardless of the dosimeter and dose rate employed and that the count rate increases with increasing dose rate and dosimeter diameter. This may indicate that a scattered gamma spectrum *Sij* is a function of the irradiation dose rate and the physical size of the

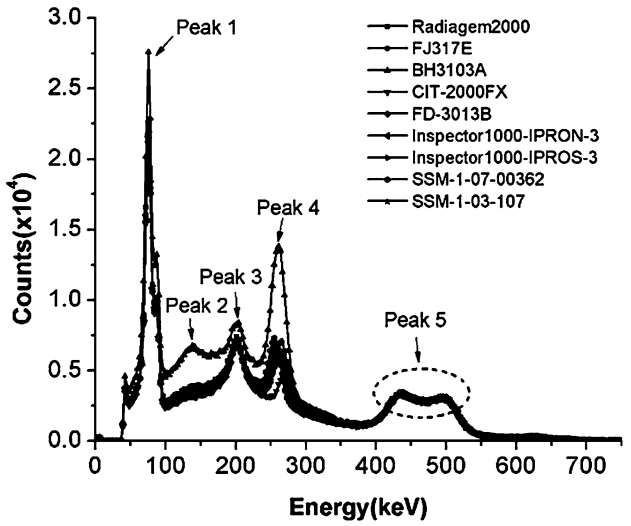

Fig. 5 Scattered gamma-ray spectra of the nine sample dosimeters irradiated with source 5

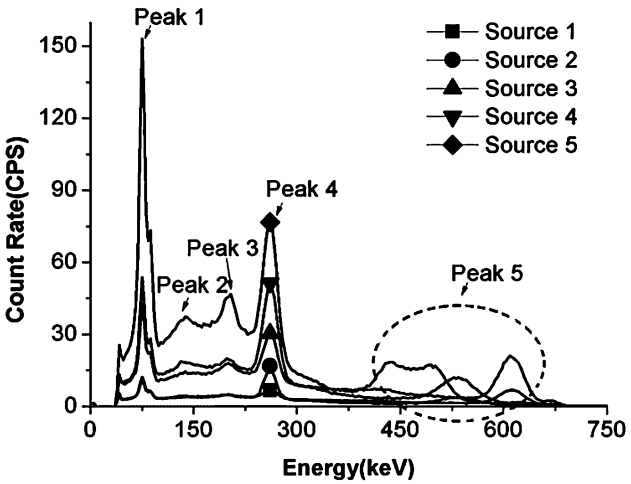

Fig. 6 Scattered gamma-ray spectra of the BH3103A probe respectively irradiated with the five sources

probes and can therefore be applied to characterize the scattered gamma-rays in the MMR.

To reduce the amount of scattering data required in the analysis, PCA was employed to extract the feature components from the spectra given in Fig. 6, and two feature components were acquired. The first component represented 81.58% of the information contained in the original spectra data, while the second component represented only 11.6%. The linear combination coefficients of the two components are shown in Fig. 7.

In Fig. 7, we note that five peaks also appear in feature component 1, with positions and shapes that are similar to those of the original scattered gamma-ray spectra. Compared to the coefficient values of the feature components shown in Fig. 8, both feature components in Fig. 7 had obvious reflex around peak 5. In addition, we note that the coefficient values of component 1 corresponding to peak 1 are far greater than those corresponding to peaks 2–4. This may indicate that the greater contribution of the source intensity to peak 1 was caused directly by characteristic X rays arising from the interaction of the irradiation with the lead shielding plates. However, this may be due to the use of only a single probe with all five sources. Figure 8 presents the two feature components extracted from the spectra given in Fig. 5. These results indicate that the contributions of peaks 1–3 are less than that of peak 4. In addition, the contribution of peak 1 is obviously decreased compared to what is shown in Fig. 7, and peak 5 has disappeared. The reason for these changes may be that only a single source was employed for all nine probes. Feature component 2, as shown in Figs. 7 and 8, also provides a meaningful contribution for characterizing scattered gamma-ray spectra in the MRR, particularly with respect to the positions of peak 4 and peak 5. Feature component 2

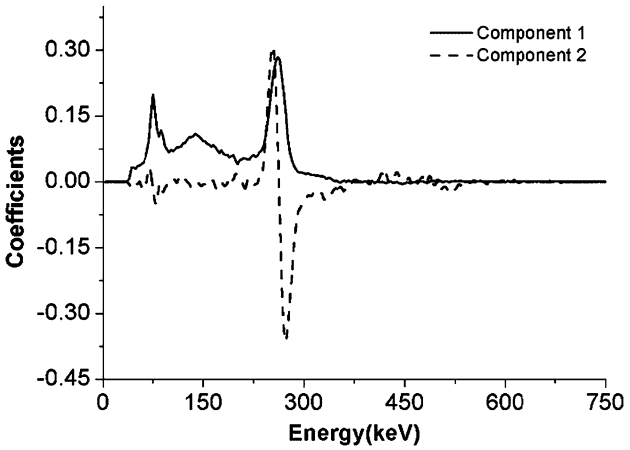

Fig. 8 Feature components of the scattered gamma-ray spectra given in Fig. 5

indicates that the information imparted by peak 4 is related more closely to the probe, while peak 5 characterizes the contribution of the irradiation source to the spectra [7]. In addition, comparison of the feature component 1 data given in Figs. 7 and 8 and the scattered gamma-ray spectrum of the BH3103A probe irradiated by source 5 is shown in Fig. 9. This data indicate that, except for the aforementioned findings, the information imparted by peak 2 is related more closely to the probes, while the information imparted by peak 3 is related more closely to the sources. Therefore, we can conclude that the feature components extracted by PCA can represent the main characteristics of scattered gamma-ray spectra separately caused by dosimeters and irradiation sources in the MRR. Extraction by PCA greatly reduces the dimensions of the original scattered gamma-ray spectra data, which is of great benefit for further data processing.

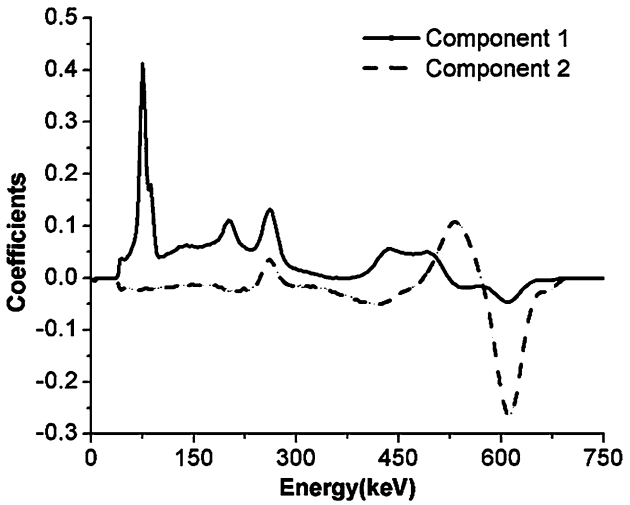

Fig. 7 Feature components of the scattered gamma-ray spectra given in Fig. 6

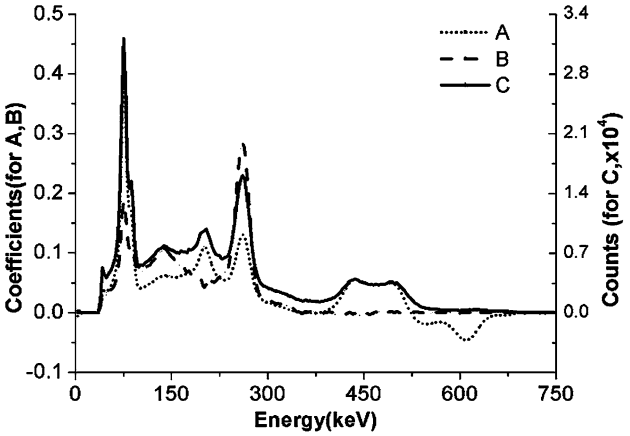

Fig. 9 Comparison of feature component 1 data extracted from the spectra given Figs. 5 and 6 and the BH3103A spectrum when irradiated with source 5: *A* feature component 1 given in Fig. 7; *B* feature component 1 given in Fig. 8; *C* the BH3103A spectrum when irradiated with source 5

4.2 Prediction results and discussion

The testing of nine dosimeters with five irradiation sources provides 5×9 sets of $Kaij'$, Sij, and $Kaij$. Selecting $E = 3$ keV for dispersing Sij provides a 512-dimension gamma-ray count rate array φijn, which can be simplified to a two-dimensional vector Ψij comprising the two feature components extracted by PCA. As discussed, LS-SVM was employed for building the prediction model $Kaij = f(\Psi ij, Kaij')$ [8–10]. We divided the 5×9 sample data sets of $Kaij'$,Ψij, and $Kaij$ randomly into training (or regression) data sets for building the model and test data sets for verifying the model's performance with a ratio of 2:1, where $Kaij$ was the output variable and $Kaij'$and Ψij were the input variables. In the course of regression, the radial basis function (RBF) was selected as the kernel function [11], and the regularization parameter c and kernel function parameter σ^2 were determined and confirmed using the 10-fold cross-validation method [12]. Finally, the following prediction model was acquired:

$$Kaij = F[(\Psi ij; Kaij'), (\Psi'), K']' \times a + b \quad (1)$$

where F is the kernel function for model regression training, Ψ' is the feature component matrix of the sample data, K' is the sample array of $Kaij$, α is the regression factor of the model, and b is the bias of the model,.

A comparison of the predicted $Kaij$ values obtained using Eq. (1) and the $Kaij$ values of the nine dosimeters determined experimentally using the five irradiation sources is presented in Fig. 10.

The training errors and the test errors were evaluated to verify the performance of the $Kaij$ prediction model. A training error was defined as the percentage difference between a predicted value of $Kaij$ and the experimentally determined value of $Kaij$ for the training data only. A test error was similarly defined for the test data only. The maximum, mean, and minimum errors obtained are presented in Table 3. Figure 11 presents the distribution of the training and test errors.

The mean square error of the 45 predictions was 4.39%, which represents the mean bias of all prediction values relative to the experimentally determined values of $Kaij$, and the maximum prediction error was less than ±10%. We may also note from Fig. 11 that the prediction errors decrease with increasing dose rate. From Fig. 11, we note that the prediction errors can be controlled within ±5% for a dose rate greater than about 393.48 Gy/h. For gamma-ray dosimeters employed for radiation protection, the relative intrinsic error of a dosimeter calibrated according to JJG393-2003 or IEC60846 cannot be greater than ±20%. The level of training error and test error demonstrated in our investigation were about ±10%, which indicates that the proposed method represents a feasible alternative to present standards employing an SRR.

Analysis reveals three main error sources. The first error source, and possibly the most prominent, was the positioning precision of the shielding box relative to their radiator and the probe position in the MRR owing to manual positioning. The second error source is the degree of representativeness and the performance of the dosimeters employed in the study. The third error source involves the viability of the feature components extracted by PCA, and the reliability of the prediction model building process.

Table 3 Training errors and test errors

Item/index	Maximum (%)	Mean (%)	Minimum (%)
Training	10.28	3.45	0.06
Test	−8.76	3.88	0.19

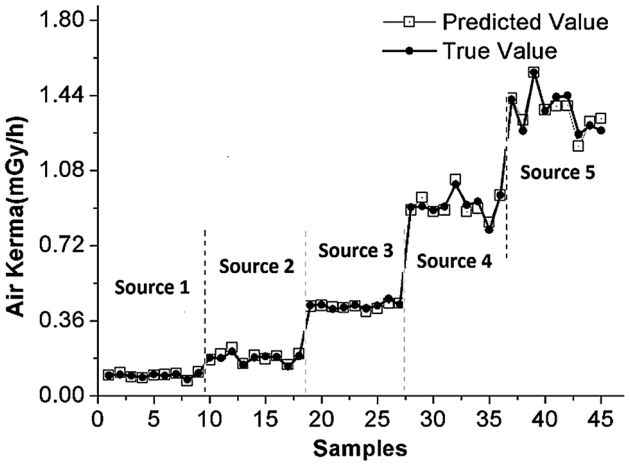

Fig. 10 Comparison of $Kaij$ values predicted by Eq. (1) and the experimentally determined true values

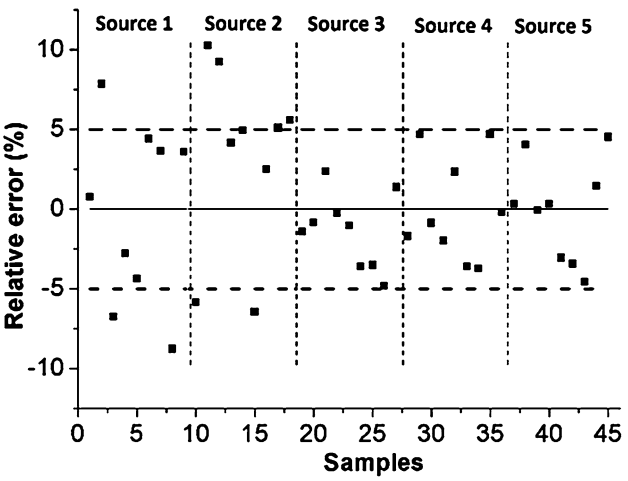

Fig. 11 Distribution of the relative errors for all samples

It is expected that all three of these error sources are amendable to improvement.

5 Conclusion

The primary results of this study demonstrated the feasibility of determining the conventional true value of gamma-ray air kerma in a reference radiation of dimensions 1 m × 1 m × 1 m. The smaller dimensions of the MRR greatly reduce the weight to a point where mobile calibration is possible. This suggests the feasibility for calibrating dosimeters using a mobile installation, and obtaining a calibration error that is at least equivalent to that obtained using an SRR, as stipulated by ISO4037-1 or GB/T12162.1. The feature components of scattered gamma-ray spectra were extracted by PCA and were employed in the study to characterize the interference of a dosimeter probe in the radiation field. The results showed that PCA is an effective tool for extracting the primary features of the scattered gamma-ray spectra caused by probes placed in the MRR and that the use of the feature components greatly reduces the dimensions of the spectrum. We expect that a greater number of more typical dosimeter samples would enhance the representativeness of the feature components extracted. The prediction model trained by LS-SVM using data obtained from nine sample dosimeters under five different dose rates successfully determined the conventional true value of gamma-ray air kerma in the MRR. The mean prediction error was less than 5%, and the maximum prediction error was about ±10% for the sample dosimeters considered, which meets the error requirements of JJG393-2003 and IEC60846, indicating that the proposed method represents a feasible alternative to present standards employing an SRR. However, data for a greater range of dosimeters, particularly dosimeters of a type and probe diameter that differ greatly from the sample dosimeters employed in the present model building, need to be included to improve the prediction precision of the model. The present work solves a crucial obstacle by demonstrating the feasibility of calibrating dosimeters in the field using an MRR and may provide a basis for developing mobile calibration technology.

References

1. ISO4037-1. X and gamma reference radiation for calibration dosimeters and dose rate meters and for determining their response as a function of photo energy-Part 1: Radiation characteristics and production methods. 1996
2. ISO4037-2. X and gamma reference radiation for calibration dosimeters and dose rate meters and for determining their response as a function of photo energy-Part 2: Dosimetry for radiation protection over the energy ranges 8 keV to 1.3Mev and 4 MeV to 9 MeV. 1997
3. C. Gonzalo, K. Jaroslav, Air Kerma Rate estimation by means of in situ gamma spectrometry: a Bayesian approach. Appl. Radiat. Isot. **68**, 804–806 (2010). doi:10.1016/j.apradiso.2009.09.062
4. S. Wan, X.D. He, L. Fang, Distributed Brillouin fiber sensing based on spectrum line fitting and wavelet packet denoising. Opt. Commun. **285**, 4971–4976 (2012). doi:10.1016/j.optcom.2012.07.075
5. A.J. Richard, W.W. Dean, *Applied Multivariate Statistical Analysis* (Pearson Education, New York, 2007)
6. X. Xu, L. Xie, S. Wang, Multimode process monitoring with PCA mixture model. Comput. Electr. Eng. **40**, 2101–2112 (2014). doi:10.1016/j.compeleceng.2014.08.002
7. H.E. Horst, Introduction to Radiological Physics And Radiation Dosimetry: by F.H. Attix. Published by Wiley-Interscience (1986), ISBN 0471011460607. Int. J. Radiat. Appl. Instrum. Part A. Appl. Radiat. Isot. **38**,163 (1987). Doi: 10.1016/0883-2889(87)90017-7
8. J.A.K. Suykens, J. Vandewalle, Least squares support vector machines classifiers. Neural Netw. Lett. **19**, 293–300 (1999)
9. D. Çalişir, E. Dogantekin, A new intelligent hepatitis diagnosis system: PCA-LSSVM. Expert Syst. Appl. **38**, 10705–10708 (2011). doi:10.1016/j.eswa.2011.01.014
10. Y. Zhang, Y. Qin, Z.Y. Xing et al., Roller bearing safety region estimation and state identification based on LMD-PCA-LSSVM. Measurement **38**, 10705–10708 (2013). doi:10.1016/j.measurement.2012.11.048
11. N. Cristianini, T.J. Shawe, *An Introduction to Support Vector Machines and Other Kernel Based Learning Methods* (Cambridge University Press, Cambridge, 2000)
12. S. Li, L.K. Dai, Classification of gasoline brand and origin by Raman spectroscopy and a novel R-weighted LSSVM algorithm. Fuel **96**, 146–152 (2016). doi:10.1016/j.fuel.2012.01.001